Output Observer Based Feedback for Soft Landing of Electromechanical Camless Valvetrain Actuator[1]

Katherine Peterson, Anna Stefanopoulou
Mechanical Engineering Department
University of Michigan, Ann Arbor

Tom Megli, Mohammad Haghgooie
Scientific Research Laboratory
Ford Motor Company, Dearborn

Abstract

Electromechanical valvetrain (EMV) actuators can replace the camshaft allowing for electronically controlled variable valve timing (VVT) on a new generation of engines. Before EMV actuators can be used in production vehicles two critical problems need to be resolved. First, impact velocities between the valve, valve seat, and the actuator itself need to be small to avoid excessive wear on the system and ensure acceptable levels of noise. Second, the opening and closing of the valve needs to be both fast and consistent to avoid collision with the piston and to reduce variability in trapped mass. This paper presents an observer based output feedback controller designed to achieve these goals. Theoretical analysis and experimental results of the controller are provided. The experimental results show a factor of six reduction in impact velocity and consistent and quick valve timing.

1 Introduction

The modern automotive powertrain has seen significant changes since the first Model-T came off the assembly line. Where once all operations were controlled through mechanical linkages, many powertrain systems are now controlled by electronic means. Typical examples are the spark timing, fuel injection, and recently, electronic throttle. The trend to replace mechanical systems with their digital counterparts has resulted in improved performance, fuel economy, and reduced emissions. In the effort to achieve further performance enhancements it has been proposed to replace one of the last mechanical systems left in the automotive powertrain, the fixed camshaft.

The conventional camshaft uses a fixed or variable cam profile to achieve a reasonable compromise between idle speed stability, fuel economy, and torque performance. Significant improvements in engine performance can be achieved through individual control of the valve timing. The electromechanical valvetrain (EMV) actuator has been selected as a promising solution to achieve variable valve motion and bring camless engines to the market. Currently, different versions of the EMV actuator are under development at several major automotive manufactures. As shown in Figure 1, the actuator consists of an armature driven between two extreme positions under the forcing of a set of springs and electromagnets. Initially the armature is held in one of the extreme positions by an electromagnet. The voltage across the coil is then reduced to zero and the armature is released. The springs drive the armature across the gap which in turn moves the valve. The armature is then brought to and held in the other extreme position by the opposite electromagnet.

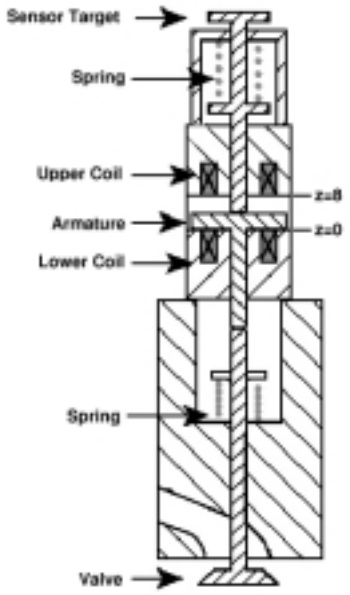

Figure 1: Electromechanical Valvetrain Actuator

The EMV actuator suffers from large impact velocities between the valve, valve seat, and the actuator itself during operation. These large impact velocities result in unacceptable noise and wear on the system. The desired impact velocity is 0.05 m/s. This velocity needs to be achieved with consistent transition times of approximately 4 ms. Consistent and quick transition times are necessary to avoid collisions with the piston and minimize variability in trapped mass. In [7] we have demonstrated the limitations of open loop (feedforward) voltage control in achieving the above requirements robustly.

This problem has been dubbed "the robust soft landing of the EMV actuator" and has attracted a lot of attention during the last three years with over twenty patents issued, and hundreds of others pending, dealing with the impact issue alone. Many of these clever mechanisms show promising results, but they typically involve complex configurations and expensive components [2]. Moreover, most of these mechanisms achieve low contact velocities by slowing down the transition time. Instead we have chosen to concentrate on a feedback control solution. The challenges are:

- Presence of significant nonlinearities in the magnetic force.

[1]Support is provided by the National Science Foundation under contract NSF-ECS-0049025 and Ford Motor Company through a 2001 University Research Project.

- Low actuator bandwidth due to the use of inductive magnetic coils.
- Robustness concerns due to low authority of the electromagnets at large distances.

Various approaches have been proposed so far. In [3] the authors use an observer based output feedback to stabilize the system and then an iterative learning controller (ILC) to achieve the desired performance. The feedback portion of the controller is not well tuned and instead relies upon the ILC to achieve the desired performance. We demonstrate here that the performance of the closed loop system can be improved with the newly designed feedback presented below. The authors of [5] use a well tuned PD controller to achieve the desired contact velocity. The transition times, however, are roughly a factor of three too large. Both the desired impact velocity and transition time are achieved in [1]. The performance is achieved by holding the ratio of the rate of change of current to current at a predefined constant. While this is effective under laboratory conditions, the authors point out potential problems when the system experiences large disturbances. In this paper we present an observer based output feedback controller to stabilize the system and provide significant performance improvements. This controller will be integrated with a cycle-to-cycle learning scheme in future work.

2 Control Architecture

We have designed and implemented a feedback controller based on sensing the position of the armature extension as shown in Fig. 1. The controller and observer output injection gains are based on linear control design methodologies. Linearizing the nonlinear model presented in [6] at two different equilibrium points we are able to approximate the nonlinear dynamics over the entire range of motion (Section 4). To overcome the inherent lag of the current caused by the inductance of the magnetic coils, it is necessary to increase the current while the armature is away from the contact position. However, closed loop control during this period has to be carefully designed to aviod unnecessarily large control signals, as the electromagnetic force has weak authority at large distances. For this reason the authors in [3] use an open loop preset voltage to avoid actuator saturation. This is not a robust approach due to varying disturbances on the valve caused by gas forces. To overcome this limitation the authors of [3] use the ILC to adjust the preset voltage from cycle to cycle.

Improved performance during a single cycle can be achieved by designing two controllers with two different objectives, switching between them at appropriate armature positions. The weighting matrix in the LQR optimization is chosen to penalize deviations from the nominal catching current much more than deviations in position or velocity. The closed loop controller is thus designed to bring the current to the nominal catching value while adjusting the voltage input depending on both the velocity and position, allowing for more robust control, while avoiding actuator saturation. When the armature is near the contact position the controller switches to a second feedback where the weighting matrices have been chosen to ensure the armature contact with the coil, i.e. regulation at the extreme position. The second feedback is designed using a reduced order model, derived from singular perturbations, to allow better controller gain selection. The controller design is presented in Section 5. In Section 6, we also decompose the weakly observable system and use an extended Kalman filter for its observable states and an open loop estimator for the weakly observable state based on the nonlinear model designed in [6]. Numerical and experimental results are shown in Section 7.

3 Nonlinear Model

The complete nonlinear state space equations describing the model are presented in [7]. The system consists of four states, namely, armature position (z in mm), armature velocity (v in m/s), upper coil current (i_u, in A) and lower coil current (i_l, in A). Due to the use of a reverse polarity voltage to achieve fast release, described in [7], the releasing coil has little influence over the armature motion. It can therefore be assumed that the magnetic force drops to zero instantly when the armature is released. Thus, only a three state model is used for controller design: armature position (y), armature velocity (v), and the catching coil current (i). The input is the catching voltage V_c in Volts. To simplify computations the armature position z is measured from the catching coil (distance) instead of its equilibrium point as in [6, 7]. Thus, the armature moves from z=8 mm to z=0 mm, The valve opening and closing directions are treated as identical here, thus, the z axis is flipped when changing between valve closing and opening.

The one-sided nonlinear state space equations derived in [6] are

$$\frac{di}{dt} = \frac{V_c - ri + \chi_1(z,i)\,v}{\chi_2(z)} \quad (1)$$

$$\frac{dz}{dt} = 1000v \quad (2)$$

$$\frac{dv}{dt} = \frac{1}{m}\left(-F_{mag}(z,i) + k_s(4-z) - bv\right) \quad (3)$$

where

$$\chi_1 = \frac{2k_a i}{(k_b+z)^2},\ \chi_2 = \frac{2k_a}{1000\,(k_b+z)}, \quad (4)$$

$$\text{and}\quad F_{mag} = \frac{k_a i^2}{(k_b+z)^2}. \quad (5)$$

For convenience, the overall system is written compactly as

$$\frac{dx}{dt} = f(x, V_c), \text{ where, } x = \begin{bmatrix} i & z & v \end{bmatrix}^T. \quad (6)$$

The system parameters used in equations (1) through (5) are defined as the resistance r in Ω, the system mass m in kg, the spring stiffness k_s in N/mm, the damping b in Ns/m. The magnetic system constants k_a and k_b are identified in [6]. F_{mag} is the magnetic force, $\chi_1 v$ is the back emf, and χ_2 is the coil inductance.

In [6, 7] the magnetic subsystem is characterized by two distinct behaviors depending on the flux-current relationship. The boundary of the two regions is defined by the

saturation current i_x which is a function of the air-gap distance. When the coil current is less than a saturation level ($i < i_x$); current and the magnetic flux are linearly related. This defines the "linear region" where equations (4) to (5) are valid. If the coil current is greater than the saturation level ($i > i_x$) then the magnetic subsystem is described by another set of equations and this defines the saturation region.

Figure 2 shows the magnetic force as a function of position for several values of current. The spring force is also plotted in Figure 2. The discontinuity in the slope of the other three force curves is a result of the saturation region, as the authors of [6] only ensured C^o continuity of their equations.

The equilibrium position is the point of intersection between the magnetic and spring force for some constant current. Analysis of the system equations demonstrates that all the equilibria near $z = 0$ are unstable, whereas, the equilibria near the middle position are stable. A perturbation from this equilibrium which decreases z will accelerate the armature toward the coil seat because the magnetic force increases parabolically while the spring force increases linearly. This acceleration can result in high contact velocities if the current is not rapidly adjusted to a lower value. On the other hand, a perturbation which increases z will reduce the magnetic force and the spring will therefore push the armature toward the middle position.

The controller goal is to drive the armature to the catching coil. The equilibrium point is given by $z_e = 0$, $v_e = 0$, and i_e. The equilibrium current, i_e, is defined as the current that gives rise to a magnetic force that exactly cancels the spring force at $z = 0$ (i.e. $F_{mag} = 4k_s$). Note here that due to the normal force acting on the armature during contact from the rigid boundary of the catching coil any current greater than i_e is also an equilibrium point. The smallest force curve is the magnetic force corresponding to i_e.

From this figure we can see that linearizing the system at i_e will cause the linear model to be highly unstable as the magnetic force drops off to much less than the spring force for just a small deviation in position. A higher value of equilibrium current will result in a linear open loop unstable system that is (i) a better approximation of the nonlinear system behavior, and (ii) a safer equilibrium point since it can account for small normal contact forces during potential bouncing.

4 Linear Model

It is desired to apply closed loop control for the majority of the armature motion, thus, a second linearization is required to approximate the armature motion away from the contact position. Linearizing near the middle position provides an accurate linear model for this purpose. For reference later, we will henceforth refer to the two linear models as

- **near model**, which is valid for $z \in (0, 1)$ mm.
- **far model**, which is valid elsewhere.

Figure 3 shows the simulation results and comparisons of

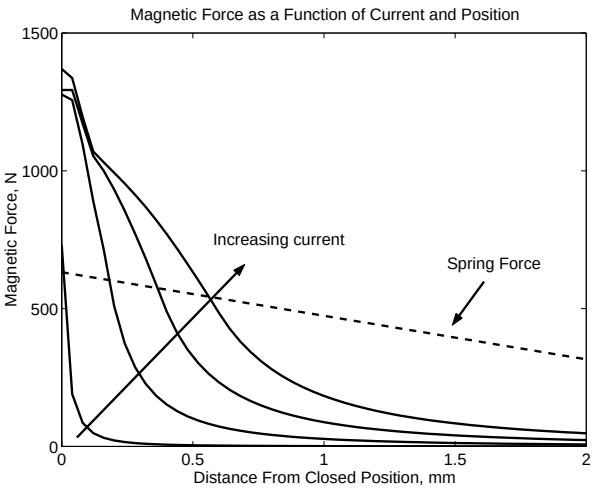

Figure 2: Magnetic Force as a Function of Position for Several Values of Current

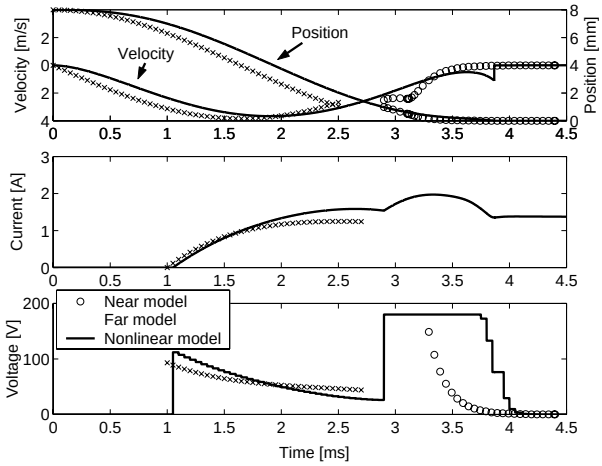

Figure 3: Comparison of the Linear and Nonlinear Models

the stabilized closed loop system of the two linear models versus the closed loop system of the nonlinear model. The same controller is employed for these simulation. Note here that the open loop near model is unstable, thus this comparison is by necessity closed loop. The current response is not plotted for the near model because the state has been removed via a model reduction derived through singular perturbations. The closed loop controller and the model reduction will be explained later in Section 5.1.

It is important to realize that even though the open loop near model has unstable dynamical behavior the armature motion is always bounded between the two electromagnets. Additionally, if a constant voltage greater than some value $V_{c\,min}$ is applied, the armature will always come to rest against the electromagnet and the current will converge to $i = \frac{V_c}{r}$. The previous result holds true for any initial conditions.

Both the near and far model have the form

$$\frac{d}{dt}\begin{bmatrix} \Delta i \\ \Delta z \\ \Delta v \end{bmatrix} = \begin{bmatrix} a_{11} & 0 & a_{13} \\ 0 & 0 & a_{23} \\ a_{31} & a_{32} & a_{33} \end{bmatrix}\begin{bmatrix} \Delta i \\ \Delta z \\ \Delta v \end{bmatrix} + \begin{bmatrix} b_1 \\ 0 \\ 0 \end{bmatrix}\Delta V_c$$

$$\frac{d}{dt}\Delta x \quad = \quad A\Delta x + B\Delta V_c$$

Note that $\frac{d\Delta i}{dt}$ does not depend on position. In reality, the rate of change of current is a function of position due to the change in inductance and back emf caused by the armature motion. The fact that $\frac{d\Delta i}{dt}$ losses the dependence on position is true for all equilibrium points. Taking the partial derivative of (1) with respect to position yields

$$\frac{\partial}{\partial z}\frac{di}{dt} = \frac{\left(v\frac{d}{dz}\chi_1\right)\chi_2 - \left(V_c - ri + \chi_1 v\right)\frac{\partial}{\partial z}\chi_2}{\left(\chi_2\right)^2} \qquad (7)$$

To satisfy equilibrium conditions

- The velocity, v, must be zero
- The Voltage V_c must equal ri

Therefore $\frac{\partial}{\partial z}\frac{di}{dt} = 0$ when evaluated at any equilibrium point. This unfortunate occurrence will only present a problem for the near model. For large values of z, the changing inductance and back emf are negligible and are of no consequence. As z approaches zero, the changing inductance and back emf are no longer negligible and must be taken into account.

5 Controller Design

The controller uses the feedback, $u = -Ke$. Where e is the error between $\widehat{x}$ and the desired equilibrium point. $\widehat{x}$ is the estimate of the actual state $x = \left[\begin{array}{ccc} i & z & v \end{array}\right]$ determined by a nonlinear state observer. The gain matrix, K, is determined by using the optimal Linear Quadratic Regulator (LQR), with diagonal weighting matrices Q and R.

As seen in Figure 2 the magnetic force is much less than the spring force for $z > 1$ mm. Therefore the actuator has low control authority over the armature motion for the majority of its travel. Additionally the magnetic coils are large inductors, resulting in a slow current response. To overcome these problems the controller is split into two stages

1. Flux Initialization controller
2. Landing controller

5.1 Stage 1 Controller, Flux Initialization

To overcome the inherent bandwidth limitations of the system, it is desired to bring the current near a nominal catching value before the armature approaches the contact position. However, closed loop control during this time may result in actuator saturation as the magnetic force has low authority for $z > 1$ mm.

To avoid this, the authors of [3] use a preset voltage when the distance is greater than a threshold value. This approach is not robust as the preset voltage can not vary to account for gas forces acting on the system. To overcome this limitation an ILC is used to adjust the preset voltage from cycle to cycle.

To improve robustness within a cycle, our controller uses the flux initialization stage to apply closed loop control for $z \in (1, 8)$ mm. Using the far model, the weighting matrix is chosen to penalize deviations from the nominal catching current much more than deviations in position or velocity. Since the actuator has control authority over current, actuator saturation is avoided. Additionally, robustness is improved as the controller can compensate for variations in both position and velocity.

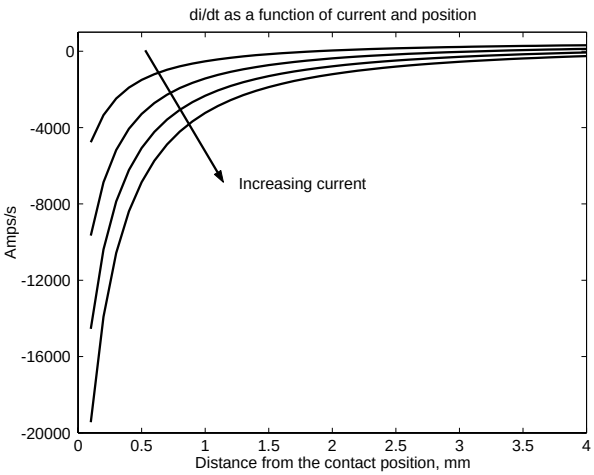

Figure 4: $\frac{di}{dt}$ as a Function of Position for Several Values of Current

3.1 Stage 2 Controller, Landing

As the armature approaches the contact position, the controller switches to the second stage at $z = 1$ mm. The landing controller catches the armature and brings it into contact with the coil while attempting to minimize the impact velocity. Control at small distances becomes very difficult due to the rapidly changing current dynamics. Combining equations (1) and (4) we obtain:

$$\frac{di}{dt} = 1000\left(\frac{\left(V_c - ri\right)\left(k_b + z\right)}{2k_a} + \frac{iv}{\left(k_b + z\right)}\right) \qquad (8)$$

As k_b is very small ($k_b << 1$) and z is approaching zero, the term $k_b + z$ is replaced with the vanishing term $\varepsilon = k_b + z$ resulting in

$$\varepsilon\frac{di}{dt} = 1000\left(\frac{\left(V_c - ri\right)\varepsilon^2}{2k_a} + iv\right) \qquad (9)$$

which we recognize as a singularly perturbed system. The singular perturbation can also be seen by plotting equation (1) against position. By assuming the velocity profile of an undamped oscillation, this has been done in Figure 4. From Figure 4 it can be seen that $\frac{di}{dt}$ does indeed approach $-\infty$ as z goes to zero.

This result does not contradict the reasoning behind the use of a flux initialization stage. The current response is slow initially, and even though it becomes faster as z approaches zero, $\frac{di}{dt}$ is negative. Therefore if the current is not bought up initially it will be extremely difficult to bring it up later in the transition.

Besides the singular perturbation, equation (9) shows that as z goes to zero the influence of the input V_c becomes very small. Therefore to drive the armature to the contact position the system will require large values of V_c. This problem will be addressed in a later paper through the use of a nonlinear feedback [4].

Unfortunately from equation (7) we know that current in the linear model completely loses its dependence on position, and thus does not capture the singular perturbation. To capture this phenomena in the linear model, we assume current has reached its quasi-steady state solution

such that

$$\frac{d\Delta i}{dt} = 0 = a_{11}\Delta i + a_{13}\Delta v + b_1 \Delta V_c \tag{10}$$

Resulting in the reduced state space representation

$$\frac{d}{dt}\begin{bmatrix} \Delta z \\ \Delta v \end{bmatrix} = \begin{bmatrix} 0 & a_{12}^* \\ a_{21}^* & a_{22}^* \end{bmatrix}\begin{bmatrix} \Delta z \\ \Delta v \end{bmatrix} \tag{11}$$

$$+ \begin{bmatrix} 0 \\ b_2^* \end{bmatrix}\Delta V_c \tag{12}$$

$$\frac{d\Delta x^*}{dt} = A^*\Delta x^* + B^*\Delta V_c \tag{13}$$

This new representation is used to design the landing controller. As the original a_{11} term is Hurwitz we need only to design a stabilizing feedback for the reduced order model.

6 Observer Design

High cost and implementation issues preclude the use of sensors to measure all three states. Instead, only a position sensor is used, and an observer is implemented to estimate velocity and current. Unfortunately, the observablility matrix

$$\begin{bmatrix} C^T & (CA)^T & (CA^2)^T \end{bmatrix}^T \tag{14}$$

where A is from the far model and $C = \begin{bmatrix} 0 & 1 & 0 \end{bmatrix}$, is ill-conditioned. Therefore one or more states are weakly observable from the position measurement. From the physics of the system it is obvious that current is the weakly observable state. For the majority of the armature travel the magnetic force, and thus current, has little influence over the armature motion (i.e. the system output). Although this is to be expected for the far model, it is important to note that using the near model will also result in an ill-conditioned observablility matrix. At small distances the magnetic force is influenced by changes in position more than changes in current. Thus the affect of current on the output is still weakly observable.

Only the far model is used to design the observer. Of the two models, the far model is valid for almost the entire range of motion. Rather than deal with the difficulties of switching between two models, the output injection term is used to ensure accuracy of the state estimates.

Setting $a_{31} = 0$, which is small in comparison to a_{32} and a_{33}, removes $\frac{d\Delta v}{dt}$ dependence's on current. The new state space matrix, $\widetilde{A}$, is given by

$$\widetilde{A} = \begin{bmatrix} a_{11} & 0 & a_{13} \\ 0 & 0 & a_{23} \\ 0 & a_{32} & a_{33} \end{bmatrix} = \begin{bmatrix} A_{\overline{o}} & A_{12} \\ 0 & A_o \end{bmatrix} \tag{15}$$

The system can now be decomposed into observable and unobservable parts, A_o and $A_{\overline{o}}$ respectively.

Using the nonlinear model presented in [6] a nonlinear exponential detector is implemented as

$$\frac{d\widehat{x}}{dt} = f\left(\widehat{x}, V_c\right) + L\left(y - \widehat{y}\right), \tag{16}$$

where, the function $f\left(\widehat{x}, V_c\right)$ is the same as equation (6) except that it does not included the saturation dynamics

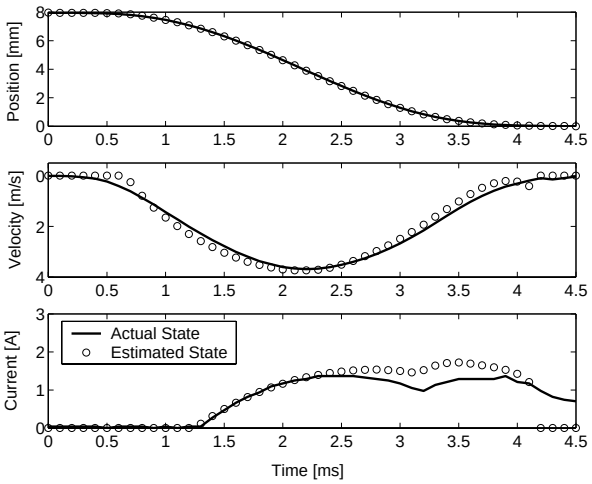

Figure 5: Comparison of the Estimated vs. Actual States

because of their lack of C^1 continuity. The matrix L is given by $L = \begin{bmatrix} 0 & l_1 & l_2 \end{bmatrix}^T$, where l_1 and l_2 are chosen by using a Kalman filter on A_o and $C_o = \begin{bmatrix} 1 & 0 \end{bmatrix}$.

A comparison of the actual and estimated states is presented in Figure 5. The observer does an excellent job of estimating both position and velocity. The current estimate matches the actual state closely for the initial part of the transition, with the error increasing toward the end. Remember that equation (16) does not include the saturation region, thus at the end of the transition when saturation occurs the nonlinear model is not accurate. Additionally the current estimate is running open loop therefore output injection can not be used to drive the error to zero. As current is not used in the landing controller stage this problem is of no consequence.

7 Results and Validation

The validation of our controller design and methodology is shown in the following performance criteria

1. Consistency between the linear and nonlinear models, shown in Figure 3.
2. Consistency between the nonlinear model and experimental results, shown in Figure 6.
3. Accurate estimation of the unmeasured states, shown in Figure 5.
4. Repeatable soft landing of the armature, shown in Figure 7 and Table 1.

A typical soft landing is presented in Figure 7. Compared to the open loop control, presented in Figure 8, the controller has achieved a significant reduction in the impact velocity. Whereas the open loop impact velocity is approximately 1 m/s the closed loop impact velocity has been reduced by a factor of six. The open loop profile was obtained by using a constant voltage input and represents the best impact velocity we could achieve with this simple input. Statistical data for the linear closed loop controller is listed in Table 1.

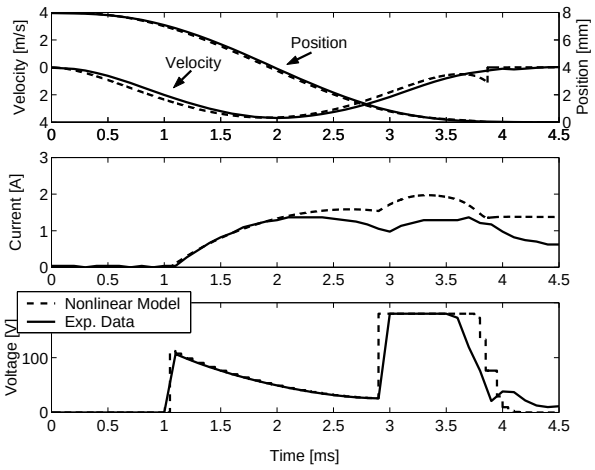

Figure 6: Comparison of the Nonlinear Model to Experimental Results

	Transition Time	Impact Velocity
Mean	3.42 ms	0.16 m/s
σ	0.2 ms	0.09 m/s
Max	4.3 ms	0.35 m/s
Min	3.3 ms	0.06 m/s

Table 1: Linear Controller Results

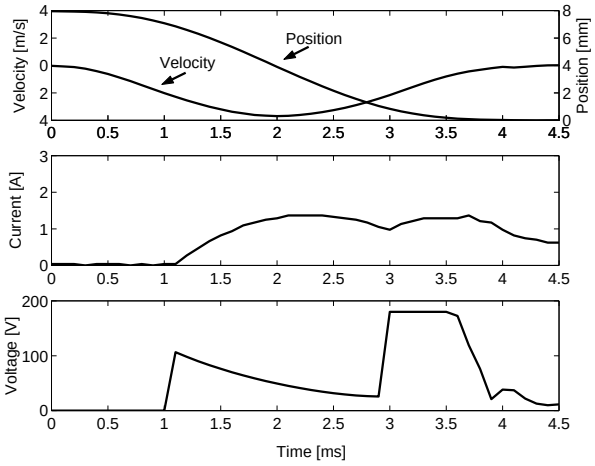

Figure 7: Typical Experimental Results

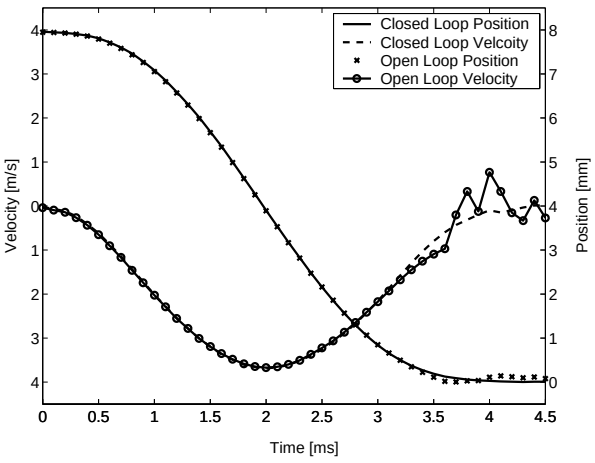

Figure 8: Comparison of the Open Loop vs Closed Loop Experimental Results

8 Conclusion and Future Work

Camless engine technology has the potential to significantly improve the modern engine. While the concept has existed for several years, the problem of ensuring accurate transitions timing with small impact velocities has prevented the technology from being implemented. Advances in control theory and microprocessor technology have allowed the potential of the system to finally be realized.

This paper has presented a linear design control methodology that reduces the impact velocities between the valve, valve seat, and the actuator. Experimental results show the controller achieves a factor of six reduction in impact velocity and consistent and quick transition times.

Future work will focus on the use of an iterative learning and nonlinear controller design. The addition of a cycle to cycle based compensation with an iterative learning controller should improve performance. As the problem is highly nonlinear, nonlinear control theory will be used more extensively in future control design. A nonlinear controller that addresses the loss of control authority has already been designed and implemented in hardware. A detailed analysis and experimental results of the nonlinear controller will be presented in a later paper [4].

References

[1] Butzmann S., Melbert J., and Koch A., "Sensorless Control of Electromagnetic Actuators for Variable Valve Train," SAE Paper No. 2000-01-1225.

[2] Flierl R., and Kluting M., "The Third Generation of Valvetrains-new Fully Variable Valvetrains for Throttle-free Load Control," SAE 2000-01-1227

[3] Hoffmann W., Stefanopoulou A., "Iterative Learning Control of Electromechanical Camless Valve Actuator," Proceedings American Control Conference, pp.2860-2866, June 2001.

[4] Peterson K., Stefanopoulou A., Wang Y., Megli T., Haghgooie M., "Nonlinear Self-Tuning Control for Soft Landing of an Electromechanical Valve Actuator," to be presented at the 2002 IFAC on Mechatronics.

[5] Tai C., Stubbs A., Tsao T.C., "Modeling and Controller Design of an Electromagnetic Engine Valve," Proceedings of American Control Conference, pp. 2890-2895, June 2001.

[6] Wang Y., Stefanopoulou A., Haghgooie M., Kolmanovsky I., Hammoud M., "Modeling of an Electromechanical Valve Actuator for a Camless Engine," Proceedings AVEC 2000, 5th Int'l Symposium on Advanced Vehicle Control, no. 93, Aug 2000.

[7] Wang Y., Stefanopoulou A., Peterson K., Megli T., Haghgooie M., "Modeling and Control of Electromechanical Valve Actuator," SAE 2002-01-1106